First-Principles Calculated Phase Diagram for Nanoclusters in the Na-Al-H System: A Single-Step Decomposition Pathway for NaAlH4

ARTICLE *in* THE JOURNAL OF PHYSICAL CHEMISTRY C · FEBRUARY 2011

Impact Factor: 4.77 · DOI: 10.1021/jp109420e

3 AUTHORS:

E. H. Majzoub
University of Missouri - St. Louis
95 PUBLICATIONS **1,628** CITATIONS
SEE PROFILE

Fei Zhou
Lawrence Livermore National Laboratory
46 PUBLICATIONS **1,655** CITATIONS
SEE PROFILE

Vidvuds Ozolins
University of California, Los Angeles
179 PUBLICATIONS **4,079** CITATIONS
SEE PROFILE

THE JOURNAL OF PHYSICAL CHEMISTRY C

ARTICLE

pubs.acs.org/JPCC

First-Principles Calculated Phase Diagram for Nanoclusters in the Na−Al−H System: A Single-Step Decomposition Pathway for $NaAlH_4$

E.H. Majzoub

Center for Nanoscience and Department of Physics and Astronomy, University of Missouri−St. Louis, St. Louis, Missouri 63121, United States

Fei Zhou and V. Ozoliņš

Department of Materials Science and Engineering, University of California, Los Angeles, California 90095-1595, United States

Supporting Information

ABSTRACT: We present first-principles calculations of the phase diagram of small clusters composed of Na, Al, and H and determine their decomposition pathways as functions of Na:Al ratio and cluster size up to eight formula units. We consider ionic clusters of AlH_3, NaH, and $NaAlH_4$ and include as decomposition products metallic clusters of Na, Al, and mixed Na−Al. Small clusters of Na_3AlH_6 are found to be unstable because of a Jahn−Teller distortion that destabilizes the constituent $[AlH_6]^{3-}$ anions and causes them to split into two H^- ions and $[AlH_4]^-$. Cluster geometries for ionic clusters were obtained by relaxing prototype electrostatic ground state (PEGS) structures using density-functional theory calculations; vibrational free energy was also calculated for each of the clusters. We find that small clusters of AlH_3 increase in stability with smaller cluster size from enthalpies of around 51 to 160 kJ/mol H_2 for eight and one formula unit (fu), respectively. In contrast, small clusters of NaH have an enthalpy of decomposition of about 70 kJ/mol H_2 and show no destabilization with size until the cluster is two formula units or smaller when they spontaneously decompose. Clusters of $NaAlH_4$ also show increasing stability with decreasing cluster size with an enthalpy of decomposition that increases from 80 kJ/mol H_2 for eight fu clusters to 150 kJ/mol H_2 for 1 fu clusters. $NaAlH_4$ clusters are found to decompose directly into mixed Al−Na clusters in one step, which is in agreement with recent experimental work on $NaAlH_4$ in nanoporous carbons. Finally, we predict destabilized reactions involving simple hydride (NaH and AlH_3) and complex hydride ($NaAlH_4$) nanoclusters that have lower critical temperatures than either of the reactants.

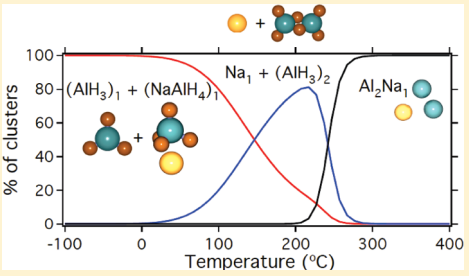

I. INTRODUCTION

Bulk solid-state reactions, such as those commonly occurring in complex-hydride-based hydrogen storage materials, present several challenges for practical applications in proton exchange membrane (PEM) fuel-cell vehicles. In contrast to the traditional interstitial metal-hydrides, which may retain their metal atom substructure upon release of hydrogen, the complex hydrides generally decompose from one or two parent solid phases into multiple product phases. These reactions typically involve breaking of covalent Al−H or B−H bonds and require large reconfiguration of structures and long-range mass transport of metal species. As a result, reaction kinetics in bulk complex hydrides are usually unacceptably slow for on-board vehicular storage. Furthermore, while the equilibrium pressure (i.e., thermodynamics) of interstitial hydrides may be easily tuned through alloying,[1] the complex hydrides are generally ionic compounds with well-defined stoichiometries that allow little alloying.[2] This results in less "tunability" of the material from an engineering standpoint.

The prototypical complex hydride that can reversibly release and absorb hydrogen is sodium alanate, $NaAlH_4$. The equilibrium decomposition reaction involves two steps as shown below.

$$NaAlH_4 \rightarrow \frac{1}{3}Na_3AlH_6 + \frac{2}{3}Al + H_2 \quad (1)$$

$$Na_3AlH_6 \rightarrow 3NaH + Al + \frac{3}{2}H_2 \quad (2)$$

The first step is decomposition into the hexahydride, Na_3AlH_6, with segregation and accumulation of bulk Al. In the second step, hexahydride further decomposes into NaH and Al. These reactions occur at modest temperatures in catalyzed $NaAlH_4$ well below the melting point of pure bulk $NaAlH_4$ at 180 °C. This material was first shown to be reversible by Bogdanovic and

Received: October 1, 2010
Revised: November 29, 2010
Published: January 25, 2011

dx.doi.org/10.1021/jp109420e | J. Phys. Chem. C 2011, 115, 2636–2643

co-workers,[3,4] who demonstrated that reversibility was possible if one added a few atomic percent of transition-metal dopants with titanium being the most effective. In a typical experiment, bulk $NaAlH_4$ is mechanically milled with a dopant precursor, such as $TiCl_3$, which disperses upon milling and results in a powder of activated $NaAlH_4$ with a particle size in the micrometer range.[5] The mechanism of action of the dopants is outside the scope of this work, however, studies indicate that small amounts of Ti affect the kinetics but not the critical temperatures of the decomposition eqs 1 and 2,[6−9] which remain too high for PEM fuel-cell vehicles.

Reducing the size of the bulk solids to the nanoscale regime is one approach that may allow for engineered equilibrium pressures and reaction kinetics that are more suitable for on-board hydrogen storage. First-principles calculations on MgH_2 nanoparticles, for example, indicate that significant lowering of the desorption enthalpy is possible with decreasing cluster size.[10] Calculations of nanocluster stability using the Wulff construction, though limited in value at very small particle size, also indicate the decreasing stability of MgH_2.[11] Recent experimental work has demonstrated considerable changes in kinetics and perhaps in thermodynamics for hydrogen storage materials when incorporated in nanoporous frameworks. These frameworks include high surface area nanoporous carbons, such as carbon aerogels,[12,13] and block-polymer-templated highly ordered carbons[14] as well as metal−organic framework (MOF) materials such as the benzene tricarboxylate-linked HKUST-1 (Cu-BTC).[15] A practical use of nanoparticle hydrides for storage applications would require a suitable framework that prevents agglomeration while preserving, as much as possible, the volumetric and gravimetric parameters of the underlying material. This poses a difficult challenge as the framework wall structure would necessarily need to be thin yet robust against reduction and mechanical degradation, for example. The results presented here are an indication of the size of the lower limit of the framework pore size only.

Calculations of sodium alanate decomposition thermodynamics for particles in the 2−10 nm range have shown that the decomposition products are NaH and Al and that hexahydride Na_3AlH_6 is bypassed in the reaction sequence because of a large surface energy.[16] Additionally, there is work using the bond-order formalism in NaH to develop potentials suitable for use in studying small clusters of $NaAlH_4$.[17] This paper addresses the intrinsic reaction thermodynamics and decomposition pathways of gas-phase sodium alanate clusters in the 1−2 nm size regime; such clusters have recently been synthesized in nanopores in refs 14, 15, 18, and 19. Using the recently developed prototype electrostatic ground state (PEGS) method in conjunction with density-functional theory (DFT) calculations, we predict the structures of small clusters of $NaAlH_4$ and its decomposition products (Al, Na, Al_mNa_n, NaH, AlH_3, and Na_3AlH_6) with up to eight Na and Al atoms. We generalize the grand-canonical linear programming (GCLP) method to determine thermodynamically preferred decomposition pathways in finite-size systems and obtain the phase diagram of small, free clusters of sodium alanate, including vibrational contributions to the free energy.[20] We find that the resulting decomposition pathways of free-standing $(NaAlH_4)_n$ clusters with $n \leq 8$ are drastically different from those of bulk sodium alanate favoring hydrogen release in a one-step reaction leading to the formation of mixed $(AlNa)_n$ nanoclusters. We also predict nanocluster analogues of bulk destabilized reactions[21−23] between simple hydride (NaH and AlH_3) and complex hydride ($NaAlH_4$) nanoclusters.

II. COMPUTATIONAL METHODS

Cluster Geometries. Nanocluster geometries for nonmetallic clusters were generated using the method of prototype electrostatic ground states (PEGS) described elsewhere.[24] Briefly, the PEGS method globally optimizes low-energy geometric configurations of a collection of charge-balanced complex anions and cations to provide structure prototypes for first-principles total energy calculations. A simplified Hamiltonian, including the electrostatic interaction of ions and soft-sphere repulsion, provides rapid evaluation of the potential energy surface and is searched using Monte Carlo random walk. The PEGS method is well established for bulk ionic solids and generally finds ground-state crystal structures.[25,26] In addition, the PEGS method is also applicable to polymorphic crystals and may be used to find high-temperature polymorphs and metastable structures.[27,28]

The computational cost for effectively searching the potential energy surface for a nanocluster is demanding. Our implementation of PEGS for nanocluster searches utilizes a novel Monte Carlo method based on a random walk in energy space first described by Wang and Landau.[29] This method avoids the common pitfall of trapping in local energy minima by using an acceptance/rejection criterion based on the density-of-states function $g(E)$, which forces the system to explore all configurations with energies below a given upper bound. The development and use of Wang−Landau Monte Carlo (WLMC) as an energy minimizer for searching low-energy configurations of clusters with Lennard-Jones, and other simplified Hamiltonians, will be described in an upcoming publication.

Aluminum hydride and sodium hydride clusters were represented as collections of positively charged cations ($Q_{Na} = +1$, $Q_{Al} = +3$) and hydrogen anions ($Q_H = -1$). The ionic radii used in the PEGS soft-sphere repulsion term were set so that interatomic distances matched those found in bulk AlH_3, $R_{Al-H} = 1.71$ Å, and NaH, $R_{Na-H} = 2.44$ Å. Sodium alanate clusters consist of Na^+ cations and rigid $[AlH_4]^-$ complex anions with fixed Al−H bond lengths of $R_{Al-H} = 1.65$ Å and hydrogen charges $Q_H = -0.6675$; charge neutrality then requires $Q_{Al} = -(1 + 4Q_H)$. These parameters have been shown to successfully predict the crystal structures of bulk alanates.[24] We limited our cluster sizes to eight formula units corresponding to the maximum diameter of $NaAlH_4$ clusters of about 8−15 Å depending on the geometry. This size is comparable to the pore size in the $NaAlH_4$-infiltrated Cu-BTC MOF in the work of Bhakta et al., which is about 15 Å in diameter.[15] We generated only stoichiometric AlH_3 clusters and did not attempt to explore other stable clusters in this area.[30]

Since PEGS is not expected to provide a reasonable description of the energetics of metallic clusters, a different approach was adopted for Al_mNa_n clusters. Starting geometries for sodium clusters were taken from de Heer,[31] while those for aluminum and mixed Al_mNa_n cluster geometries were obtained through WLMC optimization using a Lennard-Jones Hamiltonian using $\varepsilon = 1.0$ and σ such that minimum interatomic distances were $R_{Al-Al} = 2.48$ Å, $R_{Na-Na} = 3.35$ Å, and $R_{Al-Na} = 3.15$ Å. Our results for Al_n clusters are in good agreement with earlier studies (see ref 32 and refs therein). For mixed Al_mNa_n clusters with $n \neq m$, we started with optimized Lennard-Jones geometries and carried out first-principles molecular dynamics simulated annealing runs of 18 ps gradually raising temperature from 300 to 450 K and then cooling back down to 300 K. Aluminum and sodium are immiscible in the bulk equilibrium phase diagram forming phase separated Na and Al regions. The Al−Na clusters generated in this work also appear to indicate that the clusters are essentially phase separated

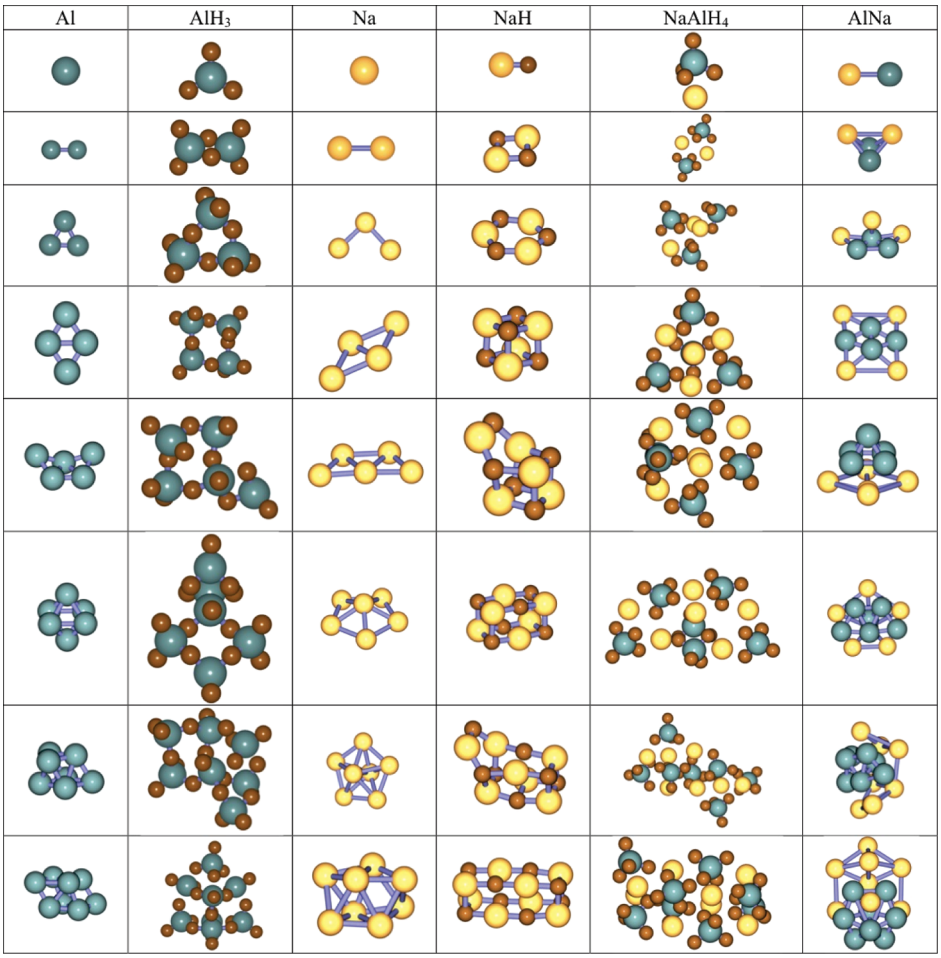

Figure 1. First-principles relaxed cluster geometries used in this work.

into Al and Na, however, the combined cluster is energetically favorable to physically separated Al and Na clusters.

All clusters were relaxed using first-principles density functional theory (DFT), as described later, followed by a DFT calculation of the vibrational mode frequencies. Cluster geometries with unstable modes were further optimized with short ab initio molecular dynamics runs at 300 °C for 3 ps, followed by relaxation, and recalculation of the vibrational frequencies. This procedure was repeated until no unstable modes were found in the phonon spectra. Final cluster geometries are shown in Figure 1 for all ionic and metallic clusters and Na:Al in a 1:1 ratio. The geometries of all clusters are shown in Supporting Information.

First-Principles Energetics. Cluster binding energies were calculated using the first-principles density-functional theory (DFT) program Vienna Ab Initio Simulation Package.[33,34] Projector augmented wave (PAW) pseudopotentials were used to represent the interactions between the ions and the valence electrons.[35,36] Electronic exchange-correlation interactions were treated in the generalized gradient approximation (GGA) using the exchange correlation functional of Perdew and Wang.[37] The 3s and 3p electrons in Na and Al and the 1s electrons in H were treated as valence. Electronic states were expanded in plane wave basis with an energy cutoff of 600 eV. All structures were relaxed using the conjugate gradient algorithm until the atomic forces were less than 0.01 eV/Å. Phonon frequencies were calculated using the supercell frozen phonon force constant method using the same PAW pseudopotentials, exchange correlation functional, and plane wave energy cutoff as in the total energy calculation. A description of this implementation and its technical details can be found elsewhere.[38] First-principles molecular dynamics runs were performed using Nose-Hoover thermostat for temperature control.[39]

Cluster Phase Diagrams and Decomposition Pathways. Theoretical description of hydrogen storage reactions in small clusters requires extension of the grand-canonical linear programming (GCLP) framework, which only applies to bulk materials. The GCLP method, first proposed by Akbarzadeh et al. in their treatment of the Li−Mg−N−H system,[20] uses the Gibbs free energy of a system in contact with a reservoir of gaseous hydrogen to determine the equilibrium phases at a given temperature and pressure. For each temperature, one scans over the compositions of non-hydrogen species (i.e., Na and Al) and minimizes the free energy to determine the equilibrium phase fractions; changes in the phase fractions at two successive temperatures are used to rigorously identify all thermodynamically reversible hydrogen storage reactions.[26,40,41] In bulk systems, the unknown phase fractions are real numbers between 0 and 1, and the minimization of the free energy can be performed using standard linear programming methods. In contrast, linear programming cannot be used to find the equilibrium state of finite cluster systems because of the discreteness of the composition space. Furthermore, statistical fluctuations in the number of hydrogen

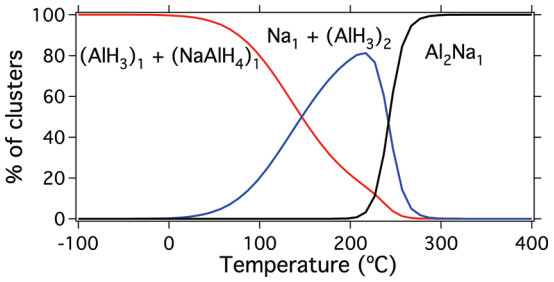

Figure 2. Calculated cluster probabilities for $N_{Al} = 2$ and $N_{Na} = 1$ as functions of temperature at $p = 0.01$ bar H_2 pressure.

atoms play an important role in finite clusters and lead to the coexistence of hydrogen-rich and hydrogen-poor clusters.

Consider an ensemble of finite systems in contact with a reservoir of gaseous hydrogen where each system is required to contain exactly N_s atoms of each non-hydrogen species (i.e., Na and Al), while the number of hydrogen atoms can vary. In each system, the constituent atoms are allowed to assume any configuration that consists of clusters of different sizes as long as they sum up to the required values of N_s. Mathematically, each possible configuration is described by nonnegative integer variables y_i^f, which give the number of clusters of type i in configuration f. There are constraints on the allowed values of y_i^f:

$$N_s = \sum_i y_i^f n_i^s \tag{3}$$

ensuring a fixed composition of non-hydrogen species. The probability of finding any given configuration f is

$$p_f = \frac{1}{Z} e^{-1/k_B T \sum_i y_i^f [F_i(T) - \mu_H(p,T) n_i^H]} \tag{4}$$

where $F_i(T)$ is the free energy of cluster i, including vibrational contributions. The number of hydrogen atoms in cluster i is given by n_i^H, and the chemical potential of gaseous hydrogen as a function of pressure and temperature is given by $\mu_H(p,T)$. The partition function Z is calculated by summing over all configurations that are consistent with the constraints given by eq 3:

$$Z = \sum_f e^{-1/k_B T \sum_i y_i^f (F_i - \mu_H n_i^H)} \tag{5}$$

In practical calculations, the number of possible configurations that satisfy eq 3 is very large, and it is convenient to impose an additional constraint:

$$\sum_i y_i^f \leq 2 \tag{6}$$

ensuring that each configuration contains no more than two clusters; this condition excludes high-energy configurations that are fragmented into many small clusters.

The scheme defined by eqs 3−6 presents a general statistical method for determining phase equilibria in finite hydride clusters. Typical results of such calculations are shown in Figure 2 for the case $N_{Al} = 2$ and $N_{Na} = 1$. Using a hydrogen pressure of $p = 0.01$ bar, which is typical for experimental measurements in the current literature, we obtain that at low temperatures the probability of finding a fully hydrogenated mixture of $(AlH_3)_1$ and $(NaAlH_4)_1$ is 100%, while at high temperatures, the fully dehydrogenated Al_2Na_1 cluster is stable. In the temperature window between approximately 100 and 250 °C, the $(AlH_3)_2$ cluster is intermittently stable, but there is a transition region of finite width where the probabilities of finding $(AlH_3)_1$, $(NaAlH_4)_1$, and Al_2Na_1 clusters vary smoothly between 0 and 1. This region should be interpreted in a probabilistic sense, where each system fluctuates between the hydrogenated and (partially) dehydrogenated states by absorbing and releasing hydrogen from the gas phase.

Broadening of Critical Temperatures. An important effect of finite size is to broaden the temperature range over which hydrogen is released from or absorbed by the cluster (see Figure 2). We define a critical temperature T_c where the free energies of the hydrogen-rich reactants and hydrogen-poor products are equal. The Gibbs free energy difference between the clusters is given by

$$\Delta G = \Delta H - T\Delta S = F_r - F_p - (n_r^H - n_p^H)\mu_H(p,T) \tag{7}$$

where the subscripts r and p label reactants and products, respectively. We assume that the entropy change ΔS is dominated by the gas-phase entropy of H_2, $\Delta S = {}^1/_2(n_r^H - n_p^H)S_{H2}$, where S_{H2} is the entropy of gaseous H_2, and we neglect the temperature dependence of ΔH and ΔS around the critical temperature T_c. The probabilities are found from eqs 4 and 5:

$$p_r = \left[1 + \exp\left(\frac{\Delta G}{k_B T}\right)\right]^{-1} \qquad p_p = 1 - p_r \tag{8}$$

Obviously, at $T = T_c$, we have $\Delta G = 0$ and equal probabilities for both clusters, $p_r = p_p$. The probability of finding a hydrogen-rich cluster decays exponentially above T_c (where $\Delta G > 0$), while the probability of obtaining the dehydrogenated cluster (p_p) decreases exponentially below T_c (where $\Delta G < 0$). The width of the temperature window where both clusters can be found with appreciable probabilities can be defined as that when the probability p_r decreases to a value $1/(1 + e^3) \approx 5\%$ corresponding to $\Delta G/k_B T_{5\%} = 3$. Using eq 8 for the free-energy change ΔG, we get, with $\Delta T = T_{5\%} - T_c$,

$$\frac{\Delta T}{T_c} = \frac{2k_B}{(n_r^H - n_p^H)S_{H_2}} \tag{9}$$

The width of the transition region, as a fraction of T_c, decreases as the inverse of the number of H_2 molecules released in the reaction.

Integer Optimization of Free Energy. We find that the results of the statistical method defined by eqs 5−8 are qualitatively similar to those found from the following simplified thermodynamic treatment especially for the larger clusters. As the starting point, we adopt the Gibbs free energy shown in eq 10. Similar to eq 3, the cluster free energies are given by $F_i(T)$, and the number of hydrogen atoms in cluster i is given by n_i^H. The chemical potential of gaseous hydrogen as a function of pressure and temperature is $\mu_H(p, T)$. We introduce variables x_i, which give the number of clusters of type i present at a given pressure and temperature. The free energy is given by summing over all possible clusters:

$$\Xi(p,T) = \sum_i x_i F_i(T) - \mu_H(p,T) \sum_i x_i n_i^H \tag{10}$$

and is consistent with a given total number of non-hydrogen

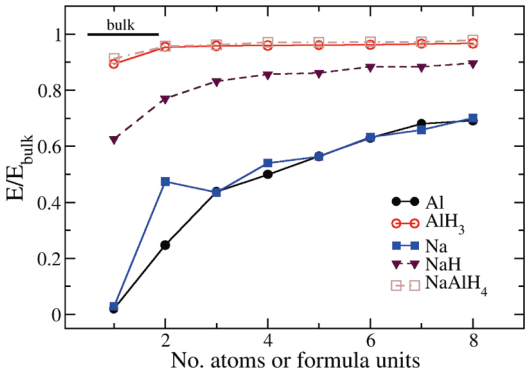

Figure 3. The first-principles total energy [without zero-point energies (ZPE)] of metallic and nonmetallic small clusters normalized to bulk values.

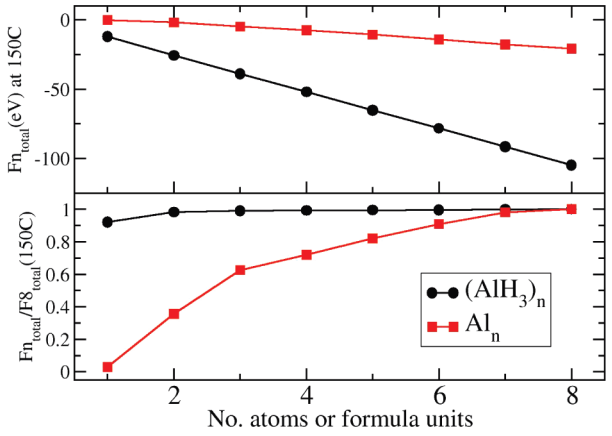

Figure 4. The top panel shows the total free energy for clusters of Al and AlH_3 at 150 °C. The bottom panel shows the change in total free energy at 150 °C normalized to an eight fu cluster.

atoms:

$$N_s = \sum_i x_i n_i^s = \text{const} \qquad (11)$$

where n_i^s is the number of atoms of type s (Na or Al) in cluster i.

In what follows, the phase diagrams of Na−Al−H nanoclusters were calculated for a hydrogen pressure of $p = 0.01$ bar since most desorption experiments on nanoporous infiltrated frameworks in the literature are performed under comparable vacuum conditions.

III. RESULTS AND DISCUSSION

The decomposition products for $NaAlH_4$ were from one to eight formula unit clusters of Al, Na, Al_mNa_n, AlH_3, NaH, Na_3AlH_6, $NaAlH_4$, and hydrogen gas. $NaAlH_4$ clusters were included in the event so that $(NaAlH_4)_8$ might decompose into $(NaAlH_4)_6 + 2NaH + 2AlH_3$, for example. Our first finding concerns the instability of small clusters of Na_3AlH_6. In all cases, we found that PEGS-generated prototype structures whose geometries were optimized using conjugate gradient relaxation via first-princples DFT would immediately transform into mixed clusters of NaH + $NaAlH_4$. For clusters up to eight fu, the AlH_6 anions in Na_3AlH_6 appear to be unstable because of a Jahn−Teller distortion arising from an accidental degeneracy of the A_{1g} and E_g electronic states at the HOMO level in $[AlH_6]^{3-}$.[42] If allowed to relax, the resulting Jahn−Teller distortion destroys the octahedral symmetry of the anion and leads to its decomposition and to a large lowering of the total energy (by a few eV per anion). In bulk crystals, this accidental degeneracy is removed by structural distortion of the AlH_6 octahedra and electrostatic crystal field effects, which combine to open a DFT band gap of approximately 2.5 eV. To find nanoclusters with stable $[AlH_6]^{3-}$ anions, we have used both PEGS searches and DFT molecular dynamics simulated annealing runs; in all cases, we observed that $[AlH_6]^{3-}$ breaks up into two H^- ions and one $[AlH_4]^-$ complex. From these results, we conclude that the lower limit on the stability of Na_3AlH_6 is somewhere above eight formula units. Therefore, in our calculations of the phase diagram, we do not predict Na_3AlH_6 as an intermediate in the decomposition process. These results are in agreement with recent experimental data on the phase diagram of Na−Al−H in nanoporous carbons.[43]

Table 1. Decomposition Temperatures and Enthalpies at P = 0.01 Bar for Small Clusters of AlH_3[a]

T [°C]	ΔH [kJ/mol H_2]	reaction
589	161	$(AlH_3)_1 \rightarrow (Al)_1 + 1.5H_2$
601	149	$(AlH_3)_2 \rightarrow (Al)_2 + 3.0H_2$
388	105	$(AlH_3)_3 \rightarrow (Al)_3 + 4.5H_2$
294	92	$(AlH_3)_4 \rightarrow (Al)_4 + 6.0H_2$
199	77	$(AlH_3)_5 \rightarrow (Al)_5 + 7.5H_2$
114	61	$(AlH_3)_6 \rightarrow (Al)_6 + 9.0H_2$
50	52	$(AlH_3)_7 \rightarrow (Al)_7 + 10.5H_2$
43	51	$(AlH_3)_8 \rightarrow (Al)_8 + 12.0H_2$

[a] Small clusters are inherently stable, in contrast to bulk AlH_3, and increase in stability with smaller cluster size.

Figure 3 shows the first-principles calculated total energies (ignoring ZPE) of several metallic and ionic small clusters normalized with respect to their bulk values. Generally, small metal clusters deviate by much larger energies than ionic clusters. The behavior of small clusters of Na is understood in terms of a well-known ellipsoidal shell model.[31] For simple decomposition reactions such as $(AlH_3)_1 \rightarrow Al + {}^3/_2H_2$, the high-energy cost of forming a free Al atom shifts the equilibrium to the left, stabilizing AlH_3. With the addition of entropy contributions, the shift because of the high-frequency Al−H vibrations is still present as shown in Figure 4, where the Al and AlH_3 cluster total free energies are referenced to eight atoms and eight formula units, respectively. The trend for all AlH_3 clusters is shown in Table 1 and indicates the stability of small clusters of AlH_3 in stark contrast to bulk AlH_3, which is inherently unstable with an enthalpy of about −10 kJ/mol AlH_3.[38,44]

The decomposition enthalpy for bulk NaH is approximately 112 kJ/mol H_2.[45] Our first-principles-calculated enthalpy for bulk NaH desorption is 94 kJ/mol H_2 at T = 300 K. Decomposition enthalpies for NaH clusters are shown in Table 2. In contrast to the results for AlH_3, which becomes dramatically more stable with decreasing particle size, NaH maintains an enthalpy for decomposition around 70 kJ/mol H_2 down to two formula units. Below two fu, the cluster is unstable and spontaneously decomposes. The trend is in agreement with highly accurate diffusion quantum Monte Carlo calculations on small clusters of LiH.[46] NaH incorporated into high surface area nanoporous carbon (HSAG-500) shows a significant decrease

Table 2. Decomposition Temperatures and Enthalpies at P = 0.01 Bar for Small Clusters of NaH

T [°C]	ΔH [kJ/mol H_2]	reaction
151	71	$(NaH)_3 \rightarrow (Na)_3 + 1.5H_2$
97	68	$(NaH)_4 \rightarrow (Na)_4 + 2.0H_2$
103	69	$(NaH)_5 \rightarrow (Na)_5 + 2.5H_2$
117	73	$(NaH)_6 \rightarrow (Na)_6 + 3.0H_2$
95	66	$(NaH)_7 \rightarrow (Na)_7 + 3.5H_2$
100	69	$(NaH)_8 \rightarrow (Na)_8 + 4.0H_2$

Table 3. Decomposition Temperatures and Enthalpies at P = 0.01 Bar for Small Clusters of $NaAlH_4$

T [°C]	ΔH [kJ/mol H_2]	reaction
597	148	$(NaAlH_4)_1 \rightarrow (AlNa)_1 + 2.0H_2$
435	115	$(NaAlH_4)_2 \rightarrow (AlNa)_2 + 4.0H_2$
350	101	$(NaAlH_4)_3 \rightarrow (AlNa)_3 + 6.0H_2$
326	97	$(NaAlH_4)_4 \rightarrow (AlNa)_4 + 8.0H_2$
239	81	$(NaAlH_4)_5 \rightarrow (AlNa)_5 + 10.0H_2$
237	81	$(NaAlH_4)_6 \rightarrow (AlNa)_6 + 12.0H_2$
222	77	$(NaAlH_4)_7 \rightarrow (AlNa)_7 + 14.0H_2$
231	80	$(NaAlH_4)_8 \rightarrow (AlNa)_8 + 16.0H_2$

in the desorption temperature as shown by Adelhelm et al.[18] These authors find a maximum hydrogen release rate at a temperature of about 240 °C under 1 atm of Ar in temperature-programmed desorption in contrast to bulk NaH with a peak desorption rate at about 360 °C. This trend agrees with our prediction of reduced enthalpies in NaH nanoclusters relative to the bulk. However, wetting effects, which are not included in the present study, may further modify the hydrogenation enthalpies in Tables 1−3 by lowering the energies of NaH and Na clusters by different amounts.

Surprisingly, the decomposition of $NaAlH_4$, at a Na:Al concentration of 1:1, is predicted to proceed along a single pathway into mixed metal AlNa clusters. This differs radically from the bulk pathway because Na and Al are completely immiscible (even in the melt) in the bulk equilibrium phase diagram. The range in enthalpy for desorption is 80−150 kJ/mol H_2. This single step desorption enthalpy for small $NaAlH_4$ clusters is significantly higher than the first-principles-calculated enthalpies for the two-step decomposition of bulk with values of ΔE (no entropy contributions) for eqs 1 and 2 of 34 and 33 kJ/mol H_2, respectively.[42]

The calculated T = 0 K phase diagram of Na−Al−H clusters is shown in Figure 5a. At T = 0 K, the stable cluster types are AlH_3, $NaAlH_4$, NaH, and Na_n ($n \leq 2$); these regions are shaded light blue in Figure 5a. For pure Al or Na, the equilibrium clusters are found to be AlH_3 and NaH, respectively, as expected. For a 1:1 ratio of Na:Al, the equilibrium cluster is found always to be $NaAlH_4$. In the two-phase regions, $(NaAlH_4)_n$ is found to coexist with another cluster type. The Al-rich region of the phase diagram, below the 1:1 diagonal, indicates a mixture of AlH_3 and $NaAlH_4$ clusters, while the Na-rich area of the phase diagram indicates a mixture of NaH (or Na_n for $n \leq 2$) and $NaAlH_4$ clusters.

Predicted chemically distinct decomposition reactions are listed in Table 4, and decomposition pathways are shown in Figure 5b. We see that in addition to the one-step decomposition reactions of NaH, AlH_3, and $NaAlH_4$ clusters (reactions 1−3 in Table 4), there are seven additional reactions that involve two reactants on the left-hand side. Two of these reactions, 7 and 8, warrant special attention as they both involve sodium alanate as one of the reactants and occur over a wide composition range in Figure 5b. All of the reactions 4−8 in Table 4 are nanoparticle analogues of destabilized reactions.[21,22] Destabilization is achieved when the critical temperature of the combined reaction is lower than the decomposition temperatures of the individual reactants because of the formation of a stable low-energy reaction product. This point can be illustrated by taking reaction 8 as an example. The decomposition pathways of the reactants, $(AlH_3)_n$ and $(NaAlH_4)_m$, lead to the formation of metallic clusters of Al_n and $(NaAl)_m$, respectively. Reaction 8 can be obtained by superimposing the individual decomposition reactions 2 and 3 and subsequently merging the separated reaction products [Al_n and $(NaAl)_m$] into one Na_mAl_{n+m} cluster. The last step is highly favorable for small clusters, and the total enthalpy change per H_2 molecule in the combined reaction 8 can become lower than either of the enthalpies of reactions 2 and 3. The energy gain must be sufficiently large to drop the critical temperature of reaction 8 below those of reactions 2 and 3. This condition turns out to be satisfied over an appreciable range of particle sizes marked by pink shading in Figure 5b. Eventual destabilization of AlH_3 upon increasing cluster size eventually lowers its decomposition temperature below that of the combined reaction 8, and the decomposition proceeds in two steps by first decomposing AlH_3 (reaction 2) and then reacting the resulting Al nanocluster with $NaAlH_4$ to form a mixed Al−Na cluster.

We next turn to describing the decomposition pathways as functions of cluster composition (see Figure 5b).

a. Single-Phase Reactions. The single-phase regions in Figure 5b (shaded light blue) contain clusters of NaH, AlH_3, and $NaAlH_4$, which all decompose in one step; thermodynamics of these reactions have been discussed, see Tables 1−3.

b. Excess Aluminum. Decomposition sequence in the two-phase region where $(NaAlH_4)_m$ coexists with $(AlH_3)_n$ is determined by the competition between the decomposition reactions of the reactants (reactions 2 and 3) and the destabilized reaction 8. For the cluster sizes considered in the present study, the destabilized reaction is favored for all compositions except the special case of $(AlH_3)_1 + (NaAlH_4)_1$, which decomposes as shown in Figure 2 because of the high stability of the AlH_3 molecule.

c. Excess Sodium. In the yellow-shaded, two-phase region just below the diagonal in Figure 5b, where $NaAlH_4$ clusters coexist with Na_1 and Na_2, the decomposition proceeds in one step according to reaction 6 in Table 4 forming mixed Al−Na clusters as end products. For higher Na fraction further to the right from the diagonal, $(NaAlH_4)_m$ clusters coexist with $(NaH)_n$ and the decomposition proceeds in one step via reaction 7. However, the decomposition temperatures of $(NaH)_n$ clusters according to reaction 1 are quite close to those of reaction 7, and for some compositions, metallic Na_n clusters show up as a transient phase in a narrow temperature interval but never raise to more than 50% probability according to eq 3; in these rare cases, NaH clusters partially decompose into Na clusters, which subsequently react with alanates to form mixed Na−Al clusters.

Finally, we compare our findings with the experimental data on MOFs infiltrated with $NaAlH_4$ via a tetrahydrofuran (THF) solution method. Figure 2 in the work of Bhakta et al.[15] shows hydrogen desorption quantity and rate from both bulk $NaAlH_4$ and $NaAlH_4$ infiltrated in the HKUST-1 MOF showing that hydrogen release occurs at temperatures well below the melting

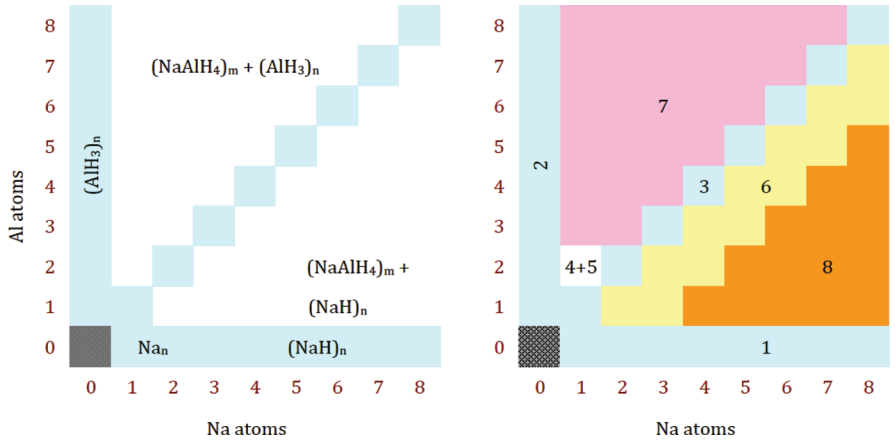

Figure 5. (a) Calculated $T = 0$ K phase diagram as a function of the number of Al and Na atoms in the cluster. Single-cluster regions are shaded blue, and regions where two clusters coexist are white. (b) Predicted $T > 0$ decomposition pathways. Reactions are numbered according to Table 4, and label "4 + 5" means that reaction 4 is followed by reaction 5 at higher temperatures.

Table 4. Predicted Hydrogen Release Reactions for Na−Al−H Nanoclusters

no.	reaction
1.	$(NaH)_n \rightarrow Na_n + (n/2)H_2$
2.	$(AlH_3)_n \rightarrow Al_n + (3n/2)H_2$
3.	$(NaAlH_4)_n \rightarrow (NaAl)_n + 2nH_2$
4.	$(AlH_3)_1 + (NaAlH_4)_1 \rightarrow (AlH_3)_2 + Na_1 + {}^1/_2H_2$
5.	$(AlH_3)_2 + Na_1 \rightarrow Al_2Na_1 + 3H_2$
6.	$Na_n + (NaAlH_4)_m \rightarrow Al_mNa_{m+n} + 2mH_2$
7.	$(AlH_3)_n + (NaAlH_4)_m \rightarrow Al_{n+m}Na_m + [(4m + 3n)/2]H_2$
8.	$(NaH)_n + (NaAlH_4)_m \rightarrow Al_nNa_{n+m} + [(4m + n)/2]H_2$

point of bulk $NaAlH_4$ at 180 °C. The only desorption product visible in this study in X-ray diffraction (XRD) was Al, which appears to have agglomerated to a particle size larger than the initial infiltrated sample on the basis of the peak width and the Debye−Scherrer particle size equation. However, one would expect that nanoparticles of Al and Na, phase-separated on the nanoscale, would be significantly dominated in XRD intensity by the Al scattering factor, which goes as Z^2. These temperatures of release trends are consistent with our calculated desorption pathways of free-standing clusters. As a word of caution, because our calculations neglect interactions with the support, the gas-phase energetics are not expected to correspond directly to the experimental results on supported clusters. Instead, they provide qualitative guidance to interpreting the experimental results and to designing optimal pore sizes and cluster compositions.

IV. CONCLUSIONS

It is not clear from current experimental data how to differentiate between the size effect on the total energy of the clusters and the interaction energy between the cluster and the porous framework. Both of these effects can change the thermodynamics and kinetics of hydrogen sorption reactions. For example, it is well established in the bulk decomposition pathway that Al phase segregates and forms Al grains of large coherence length.[4,47] By taking these materials to the nanoscale, the thermodynamics may be changed in two ways. First, as the cluster size is reduced, the metallic clusters obtain total energies per atom far larger than their bulk counterparts (see Figure 3). With respect to eq 1, this raises the total energy of the product phase Al and tends to stabilize $NaAlH_4$. The free-cluster calculations in this work address directly the change in the thermodynamics and the resulting reaction pathway of small clusters of $NaAlH_4$. The second, and more difficult, effect to quantify is the cluster/substrate interaction. The difficulty of determining cluster geometries and cluster/substrate interfaces precludes a straightforward calculation of the change in total energies of the reactant and product phases. However, it is clear that such interactions are present, for example, in the case of nanoporous carbon substrates (HSAG-500), where there is clearly a large wetting energy for molten $NaAlH_4$, as shown in recent high-pressure calorimetry measurements indicating a large exotherm on melting during the infiltration process.[18] Additionally, pressure−composition isotherms of $NaAlH_4$ incorporated into microporous activated carbon substrates display a loss of the distinct plateau indicative of the two-step process in bulk $NaAlH_4$.[48] Similar wetting exotherms are observed for $LiBH_4$ melt-infiltration into nanoporous carbons.[14]

Free-cluster calculations indicate that particle size may be a large and contributing (not necessarily dominant) factor. It is difficult in experiment to distinguish the substrate interaction from the free-cluster size effects especially when cluster sizes are small and the interaction with the substrate occurs over a larger portion of the surface area of the sample. However, it is important to know the relative magnitude of the effects (e.g., change in enthalpy) as this may allow for a more suitable choice of framework material for a given hydrogen storage compound.

In summary, we have presented a first-principles calculation of the desorption pathway of nanocluster $NaAlH_4$ into mixed metal NaAl nanoclusters. The decomposition is predicted to occur in a single step for a Na:Al ratio of 1:1 and contains no Na_3AlH_6 intermediate because of the instability of the hexahydride anion from a Jahn−Teller distortion present in small clusters. The absence of hexahydride in the decomposition pathway is in agreement with $NaAlH_4$-infiltrated nanoporous carbon desorption experiements in the literature. Small clusters of aluminum hydride are predicted to be inherently stable with increasing stability as the cluster size decreases with an enthalpy of 50−160 kJ/mol H_2. Our results further suggest that rehydriding of Al may be accomplished reversibly at relatively mild conditions if the particle size is restricted. With a suitable choice of framework, it may be possible to avoid the complicated wet chemical methods for recycling spent AlH_3.[49,50] One to two formula units of NaH

are predicted to spontaneously decompose, and those above three formula units show no destabilization with an enthalpy around 70 kJ/mol H_2. Clusters of $NaAlH_4$ show increased stability with decreasing size with a range of enthalpies of about 80−150 kJ/mol H_2. We also predict destabilized low-enthalpy reactions between simple metal hydride (AlH_3 and NaH) and sodium alanate nanoclusters, which offer a potential way of tuning reaction thermodynamics using finite size effects.

■ ASSOCIATED CONTENT

Supporting Information. This information is available free of charge via the Internet at http://pubs.acs.org.

■ ACKNOWLEDGMENT

This work was funded by the U.S. Department of Energy in the Hydrogen, Fuel Cells, and Infrastructure Technologies Program through the office of Energy Efficiency and Renewable Energy under Contract No. DE-AC04-94AL85000. F.Z. and V. O. gratefully acknowledge financial support from the U.S. Department of Energy, Office of Science, Basic Energy Sciences under grant No. DE-FG02-05ER46253. This research used resources of the National Energy Research Scientific Computing Center (NERSC).

■ REFERENCES

(1) Sandrock, G. *State-of-the-art review of hydrogen storage in reversible metal hydrides for military fuel cell applications*; Report for the office of naval research, OMB No. 0704-0188; SunaTech, Inc., 1997.
(2) Ronnebro, E. C.; Majzoub, E. H. *J. Phys. Chem. B* **2006**, *110*, 25686–25691.
(3) Bogdanovic, B.; Schwickardi, M. *J. Alloys Compd.* **1997**, *253*−*254*, 1–9.
(4) Bogdanovic, B.; Brand, R. A.; Marjanovic, A.; Schwicardi, M.; Tolle, J. *J. Alloys Compd.* **2000**, *302*, 36–58.
(5) Gross, K.; Thomas, G.; Jensen, C. *J. Alloys Compd.* **2002**, *330*−*332*, 683–690.
(6) Chaudhuri, S.; Muckerman, J. *J. Phys. Chem. B* **2005**, *109*, 6952–6957.
(7) Stumpf, R.; Bastasz, R.; Whaley, J.; Ellis, W. *Phys. Rev. B* **2008**, *77*, 235413.
(8) Liu, J.; Ge, Q. *J. Phys. Chem. B* **2006**, *110*, 25863–25868.
(9) Gunaydin, H.; Houk, K.; Ozolins, V. *Proc. Natl. Acad. Sci.* **2008**, *105*, 3673–3677.
(10) Wagemans, R.; van Lenthe, J.; de Jongh, P.; van Dillen, A.; de Jong, K. *J. Am. Chem. Soc.* **2005**, *127*, 16675–16680.
(11) Kim, K. C.; Dai, B.; Johnson, J. K.; Sholl, D. S. *Nanotechnology* **2009**, *20*, 204001.
(12) Gross, A.; Vajo, J.; Van Atta, S.; Olson, G. *J. Phys. Chem. C* **2008**, *112*, 5651.
(13) Gross, A.; Ahn, C.; Van Atta, S.; Liu, P.; Vajo, J. *Nanotechnology* **2009**, *20*, 204005.
(14) Liu, X.; Peaslee, D.; Jost, C.; Majzoub, E. *J. Phys. Chem. C* **2010**, *114*, 14036–14041.
(15) Bhakta, R. K.; Herberg, J. L.; Jacobs, B.; Highley, A.; Behrens, R., Jr.; Ockwig, N. W.; Greathouse, J. A.; Allendorf, M. D. *J. Am. Chem. Soc. Commun.* **2009**, *131*, 13198–13199.
(16) Mueller, T.; Ceder, G. *ACS Nano* **2010**, *4*, 5647–5656.
(17) Ojwang, J. G. O.; van Santen, R.; Kramer, G. J.; van Duin, A. C. T.; Goddard, W. A., III. *AIP Conf. Proc.* **2008**, *1046*, 23.
(18) Adelhelm, P.; de Jong, K.; de Jongh, P. *Chem. Commun.* **2009**, 6261–6263.
(19) Adelhelm, P.; Gao, J.; Verkuijlen, M. H. W.; Rongeat, C.; Herrich, M.; van Bentum, P. J. M.; Gutfleisch, O.; Kentgens, A. P. M.; de Jong, K. P.; de Jongh, P. E. *Chem. Mater.* **2010**, *22*, 2233–2238.
(20) Akbarzadeh, A.; Ozolins, V.; Wolverton, C. *Adv. Mater.* **2007**, *19*, 3233.
(21) Reilly, J.; Wiswall, R. *Inorg. Chem.* **1967**, *6*, 2220.
(22) Reilly, J.; Wiswall, R. *Inorg. Chem.* **1968**, *7*, 2254.
(23) Siegel, D.; Wolverton, C.; Ozolins, V. *Phys. Rev. B* **2007**, *75*, 014101.
(24) Majzoub, E.; Ozolins, V. *Phys. Rev. B* **2008**, *77*, 1–13.
(25) Ozolins, V.; Majzoub, E.; Wolverton, C. *Phys. Rev. Lett.* **2008**, *100*, 1–4.
(26) Ozolins, V.; Majzoub, E.; Wolverton, C. *J. Am. Chem. Soc.* **2009**, *131*, 230–237.
(27) Majzoub, E. H.; Ronnebro, E. C. *J. Phys. Chem. C* **2009**, *113*, 3352–3358.
(28) Seballos, L.; Zhang, J. Z.; Ronnebro, E. C.; Herberg, J. L.; Majzoub, E. H. *J. Al. Comp.* **2009**, *476*, 446−450.
(29) Wang, F.; Landau, D. *Phys. Rev. E* **2001**, *64*, 056101.
(30) Li, X.; Grubisic, A.; Stokes, S. T.; Cordes, J.; Ganteför, G. F.; Bowen, K. H.; Kiran, B.; Willis, M.; Jena, P.; Burgert, R.; Schnöckel, H. *Science* **2007**, *315*, 356–358.
(31) de Heer, W. *Rev. Mod. Phys.* **1993**, *65*, 611–676.
(32) Chuang, F.-C.; Wang, C.; Ho, K. *Phys. Rev. B* **2006**, *73*, 125431.
(33) Kresse, G.; Furthmueller, J. *J. Comput. Mater. Sci.* **1996**, *6*, 15–50.
(34) Kresse, G.; Hafner, J. *Phys. Rev. B* **1993**, *47*, 558.
(35) Kresse, G.; Joubert, D. *Phys. Rev. B* **1999**, *59*, 1758–1775.
(36) Blochl, P. *Phys. Rev. B* **1994**, *50*, 17953.
(37) Perdew, J.; Wang, Y. *Phys. Rev. B* **1992**, *45*, 13244.
(38) Wolverton, C.; Ozolins, V.; Asta, M. *Phys. Rev. B* **2004**, *69*, 144109.
(39) Nose, S. *J. Chem. Phys.* **1984**, *81*, 511. Hoover, W. *Phys. Rev. A* **1985**, *31*, 1695.
(40) Alapati, S.; Johnson, K.; Sholl, D. *J. Phys. Chem. C* **2008**, *112*, 5258–5262.
(41) Michel, K.; Akbarzadeh, A.; Ozolins, V. *J. Phys. Chem. C* **2009**, *113*, 14551–14558.
(42) Ozolins, V. O.; Majzoub, E. H.; Udovic, T. J. *J. Alloys Compd.* **2004**, *375*, 1–10.
(43) Gao, J.; Adelhelm, P.; Verkuijlen, M. H. W.; Rongeat, C.; Herrich, M.; van Bentum, P. J. M.; Gutfleisch, O.; Kentgens, A. P. M.; de Jong, K. P.; de Jongh, P. E. *J. Phys. Chem. C* **2010**, *114*, 4675–4682.
(44) Graetz, J.; Reilly, J.; Sandrock, G.; Johnson, J.; Zhou, W.-m.; Wegrzyn, J. Aluminum hydride, AlH_3, as a hydrogen storage compound. Report BNL-77336-2006; Brookhaven National Laboratories, 2006.
(45) Grochala, W.; Edwards, P. Thermal decomposition of the non-interstitial hydrides for the storage and production of hydrogen. *Chem. Rev.* **2004**, *104*, 1283–1316.
(46) Wagner, L.; Grossman, J., unpublished.
(47) Majzoub, E. H.; Gross, K. J. *J. Alloys Compd.* **2003**, *356*, 363–367.
(48) Lohstroh, W.; Roth, A.; Hahn, H.; Fichtner, M. Thermodynamics effects in nanoscale NaAlH4. *Chem. Phys. Chem.* **2010**, *11*, 789–792.
(49) Graetz, J.; Chaudhuri, S.; Wegrzyn, J; Celebi, Y.; Johnson, J. R.; Zhou, W.; Reilly, J. J. *J. Phys. Chem. C* **2007**, *111* (51), 19148–19152.
(50) Li, H.; Meziani, M. J.; Kitaygorodskiy, A.; Lu, F.; Bunker, C. E.; Shiral Fernando, K. A.; Guliants, E. A.; Sun, Y.-P. *J. Phys. Chem. C* **2010**, *114* (7), 3318–3322.